

The quiescent state broadband X-ray spectrum and variability of Mkn 421

M. Guainazzi¹, G. Vacanti¹, A. Malizia^{2,3}, K.S. O’Flaherty¹, E. Palazzi⁴, and A.N. Parmar¹

¹ Astrophysics Division, Space Science Department of ESA, ESTEC, Postbus 299, 2200 AG Noordwijk, The Netherlands

² BeppoSAX Science Data Center, Via Corcolle 19, I-00131 Roma, Italy

³ Department of Physics and Astronomy, Southampton University, SO17 1BJ, UK

⁴ Istituto per le Tecnologie e Studio delle Radiazioni Extraterrestri, CNR, Via Gobetti 101, I-40129 Bologna, Italy

Received 6 July 1998 / Accepted 16 October 1998

Abstract. The BL Lac object Mkn 421 was observed three times by the X-ray observatory BeppoSAX in consecutive days during 1997 April and May. The source was in a quiescent state, with an average 2–10 keV flux of 9.0×10^{-11} erg cm⁻² s⁻¹. Flux variation by a factor of $\simeq 2$ on timescales as short as a few 10^4 s were more pronounced in the hard (i.e. above $\simeq 3$ keV) than in the soft X-rays. The broadband (0.1–40 keV) spectrum is concave and can be most easily explained with a power-law model which steepens gradually with energy. In this framework, neither photoabsorption edges nor resonant absorption lines are required, strengthening the case against the ubiquity of such features in BL Lac objects, which had been previously suggested by *Einstein* observations. The broadband spectrum hardens with hard X-ray flux, mostly due to a flattening above $\simeq 4$ keV. This suggests that the relativistic highest energy electron distribution properties drive the X-ray spectral dynamics: either a stratification of the distribution in the jet with energy or inhomogeneities in the electron injection mechanism could be consistent with the observed variability pattern.

Key words: X-rays: galaxies – galaxies: nuclei – galaxies: jets – galaxies: BL Lacertae objects: individual: Mkn 421 – galaxies: active

1. Introduction

Mkn 421 was the first BL Lac object to be detected in X-rays (Ricketts et al. 1976). Subsequent observations have detected the source up to 100 keV (e.g.: Ubertini et al. 1984). The X-ray emission of Mkn 421 is highly variable, with distinct behavioral differences between soft and hard X-rays. In the 0.5–10 keV band the source is variable on time scales ranging from several hours to days, occasionally exhibiting large X-ray outbursts characterized by a marked hardening of the spectrum. EXOSAT observations showed that during the quiescent state the source hardens as it brightens (George et al. 1988). Giommi et al. (1990) showed that flux variations in the hard X-ray band

(0.7–8 keV) were more pronounced than those in the soft band (0.06–0.3 keV).

Observations with EXOSAT (Giommi et al. 1990), ROSAT (Fink et al. 1991) and ASCA (Kubo et al. 1998) reveal that variability of Mkn 421 in the soft X-ray band can be represented by small-amplitude variations about a quiescent level that remains temporally relatively constant. The timescale of these variations is of the order of days to weeks (George et al. 1988).

Mkn 421 has also been detected in γ -rays by Compton GRO/EGRET (Lin et al. 1996), and it was the first extragalactic source to be detected at TeV energies (Punch et al. 1992). Multiwavelength observations have shown that variability in the X-ray band is accompanied by significant variability in the TeV region, with little or no change in other wave bands (Macomb et al. 1995).

In this paper we report on three observations of Mkn 421 in 1997 April and May with the Narrow Field Instruments (NFI) on board the BeppoSAX X-ray observatory (see Table 1 for a log of the observations).

2. Observations and data reduction

The Italian-Dutch BeppoSAX X-ray observatory (Boella, Perola & Scarsi 1997a) carries four co-aligned NFI, which cover more than three decades of energy from 0.1 to 300 keV. These are:

- the Low Energy Concentrator Spectrometer (0.1–10 keV, LECS, Parmar et al. 1997);
- three identical Medium Energy Concentrator Spectrometers (1.3–10 keV, MECS, Boella et al. 1997b);
- a High Pressure Gas Scintillator Proportional Counter (4–120 keV, HPGSPC, Manzo et al. 1997).
- a collimated Phoswitch Detector System (13–300 keV, PDS, Frontera et al. 1997).

In this paper results from the LECS, MECS and PDS instruments are presented, because the HPGSPC data could not provide any significant spectral constraint. The HPGSPC is actually tuned for spectroscopy of bright sources with good energy resolution, while the PDS possesses an unprecedented sensitiv-

Send offprint requests to: M. Guainazzi (mguainaz@astro.estec.esa.nl)

Table 1. Mkn 421 observations log. Note that the LECS is only operated during spacecraft nighttime and collimated detectors spend about 50% of the time observing the background

Instrument	1997 April 29 (MJD 50567)		1997 April 30		1997 May 1	
	Count rate (Hz)	Exp. time (ks)	Count rate (Hz)	Exp. time (ks)	Count rate (Hz)	Exp. time (ks)
LECS	2.119 ± 0.0137	11.6	2.097 ± 0.0138	11.4	2.529 ± 0.0153	11.2
MECS1	0.544 ± 0.005	21.9	0.535 ± 0.005	24.0	0.633 ± 0.005	23.8
MECS2	0.797 ± 0.006	21.9	0.783 ± 0.006	24.0	0.915 ± 0.006	23.8
MECS3	0.827 ± 0.006	21.9	0.821 ± 0.006	24.0	0.970 ± 0.006	23.8
PDS	0.09 ± 0.03	11.0	0.19 ± 0.03	10.8	0.16 ± 0.03	9.1

ity in its energy band. Data were processed using the SAXDAS package (version 1.3.0). Publicly available response matrices (September 1997 release) were used.

For the imaging detectors, source spectra were extracted from regions of $8'$ and $6'$ radius, centered on the source positions in the LECS and MECS, respectively. Background spectra were extracted from blank sky fields. The background contributes less than 0.1% and 1% to the LECS and MECS full bandpass count rates of Mkn 421, respectively, and less than 10% in each energy channel even at the highest MECS bandpass energies. Background subtraction is therefore not critical for such a bright source.

PDS spectra were accumulated after excluding interval of source eclipse and each 5 minutes after a South Atlantic Geomagnetic Anomaly Passage, to avoid a gain instability due to recovery to the nominal crystal voltages after switch-on. PDS events were screened with a temperature-dependent Rise Time (RT) threshold, which allows a reduction by a factor of up to 50% of the instrumental background. Mkn 421 is detected at 8σ level in the 13–30 keV band. All spectra were rebinned in order to have at least 20 counts per channel, to ensure the applicability of χ^2 statistics. In the following, energies are quoted in the source frame and uncertainties at 90% level of confidence for each parameter (i.e.: $\Delta\chi^2 = 2.71$, Lampton, Margon & Bowyer 1976), unless otherwise specified.

3. Results

3.1. Timing analysis

In Fig. 1 the satellite orbit-averaged (i.e.: binning time 5700 s) light curves in the 0.1–3 keV (LECS) and 3–10 keV (MECS) energy ranges are shown (the energy boundaries have been chosen to sample different spectral components, see Sect. 3.2). Peak-to-peak variability by factors of 80% and 130% is evident in the 0.1–3 keV and 3–10 keV bands, respectively. The 3–10 keV/0.1–3 keV hardness ratio (HR) exhibits a much smaller ($\simeq 20\%$) dynamical range. Fig. 2 shows HR plotted against intensity (CR) and shows that the HR tends to increase with increasing intensity up to CR_{break} and then “saturates” to a constant level. If the data points in Fig. 2 are fit with a broken linear relation, $CR_{\text{break}} \simeq 0.82 \text{ s}^{-1}$.

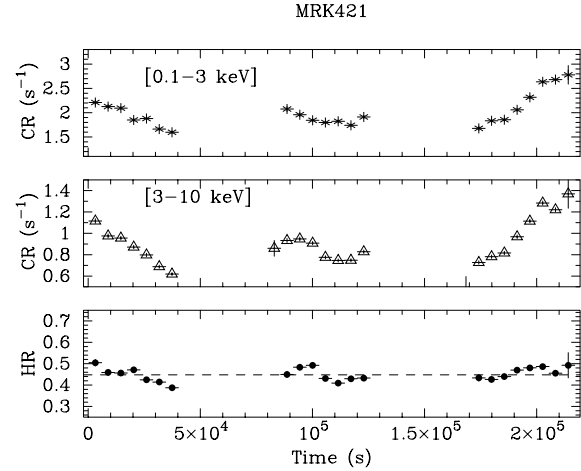


Fig. 1. Light curves in the 0.1–3.0 keV (LECS, *upper panel*), 3.0–10.5 keV (MECS, *central panel*) and their hardness ratio (HR). Binning time is 5700 s, approximately one BeppoSAX orbit. The dashed line marks the average HR

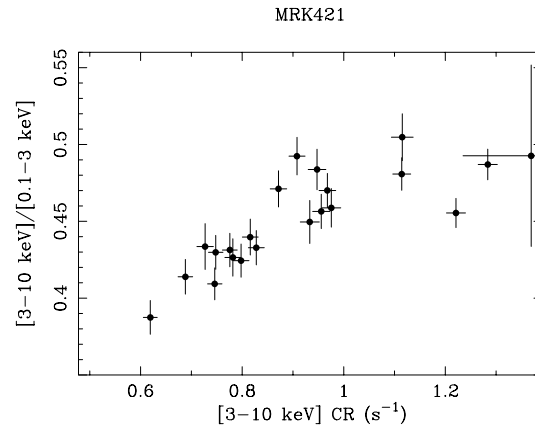


Fig. 2. Hardness ratio constructed from the 3–10 keV and 0.1–3 keV counts versus 3–10 keV count rate. Each data point corresponds to an integration time of 5700 s

This pattern of variability is typical of the quiescent X-ray state of Mkn 421 (Giommi et al. 1990; Sambruna et al. 1994). Indeed, simultaneous optical and TeV γ -ray observations of the source confirm the lack of any significant activity at the time (McEnergy & Weekes, private communication). The state

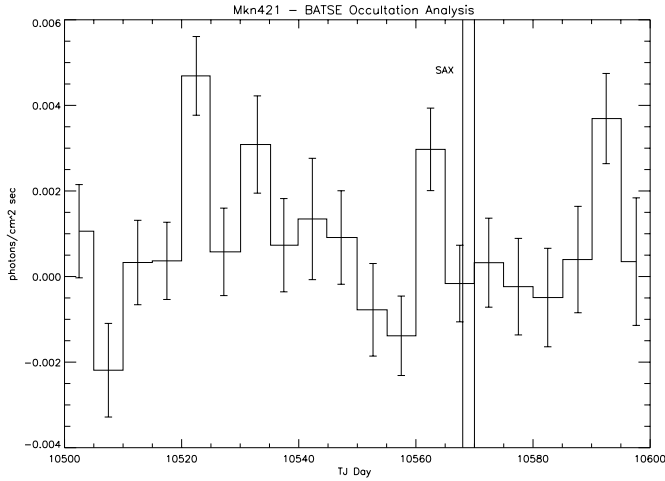


Fig. 3. BATSE light curve of Mkn 421 for the 100-day period covering the three days of BeppoSAX observation, using a bin of 5 days of the daily data. The BATSE data were collected by the Large Area Detectors in Earth occultation mode (Harmon et al. 1992). Fluxes correspond to the 20–100 keV range and have been calculated by folding a simple power-law of photon index 1.7

of quiescence is further substantiated by the BATSE light curve covering the the three days of the BeppoSAX observations (see Fig. 3). The BATSE daily monitoring sensitivity is ~ 100 mCrab, implying that sensitivities of the order of few mCrab could be achieved by integrating the data over a period of few years. Over the 100 days covering the BeppoSAX observation, the 2σ upper limit on the 20–100 keV flux was 11×10^{-11} erg s $^{-1}$ cm $^{-2}$.

3.2. Spectral analysis

Spectra from the three observations were combined, in order to maximize the signal statistics. However, given the spectral variations revealed by the timing analysis, spectral analysis was performed separately on three different data sets (a) the total time-averaged spectrum (“Phase T” hereafter); (b) a spectrum integrated over the time intervals when the 5700 s binned 3–10 keV MECS light curve has a count rate $CR < CR_{\text{break}}$ (“Phase A” hereafter); (c) the complement of Phase A (“Phase B” hereafter). Spectra from the three MECS units were summed together after gain equalization and fit together with the data from the other instruments. Data were selected between 0.1–4.0 keV, 1.8–10 keV and 13–30 keV for the LECS, MECS and PDS, respectively. Factors were included in the spectral fitting to account for known normalization uncertainties between the instruments and the PDS to MECS factor was fixed to 0.75. This value is a factor $\simeq 0.82$ lower than reported by Cusumano et al. (1998) for the Crab Nebula observation, to account for the effects of the RT screening algorithm. The following results are not affected by a residual $\sim 10\%$ uncertainty on the exact value of this parameter. The spectral results are summarized in Table 2.

The X-ray spectra of BL Lac objects are generally well described by a single power-law absorbed by an amount of matter

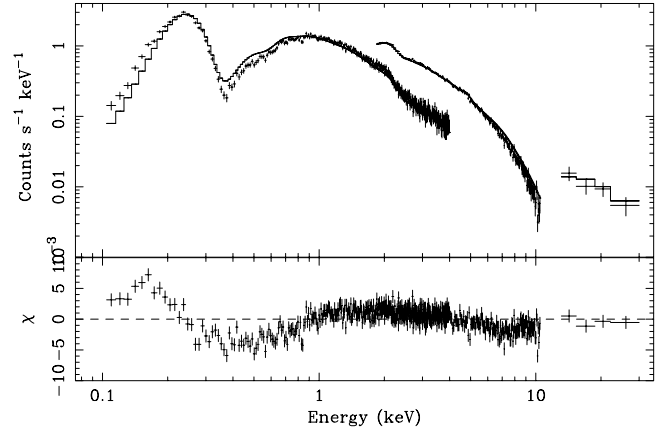


Fig. 4. Spectrum and best-fit model (*upper panel*) and residuals in units of standard deviations (*lower panel*) when the time-averaged spectrum of Mkn 421 is fit with a simple absorbed power-law model. Each data point has a signal to noise ratio > 3

consistent with the Galactic value. Some BL Lac objects, however, seem to require a model with a broken power-law, Mkn 421 being one of these (Comastri et al. 1997; Takahashi et al. 1996).

A single power-law model provides an unacceptable fit for both the total (reduced $\chi^2_{\nu}|_T = 3.26$) and the intensity resolved spectra ($\chi^2_{\nu}|_A = 1.86$; $\chi^2_{\nu}|_B = 1.86$). Fig. 4 demonstrates that this is not due to a localized feature but to an incorrect modeling of the spectrum in the whole 0.1–30 keV energy range. Although a broken power-law yields a dramatic improvement of the quality of the fit, the fit is still unacceptable for the T and B datasets ($\chi^2_{\nu}|_T = 1.28$; $\chi^2_{\nu}|_A = 1.06$; $\chi^2_{\nu}|_B = 1.21$). A good fit can be obtained if a pair of photoabsorption edges is added to the broken power-law, with threshold energies $E_{\text{th}}^1 \simeq 1.23$ keV and $E_{\text{th}}^2 \simeq 1.55$ keV. The addition of both edges is statistically required in the time-averaged spectrum ($\Delta\chi^2 = 126$ and 29 for their subsequent inclusion in the spectral model). The best-fit threshold energies are broadly consistent with those expected from highly ionized Neon species NeIX ($E_{\text{th}} = 1.19$ keV) and NeX ($E_{\text{th}} = 1.36$ keV). No Oxygen edges are, however, detected, with the 90% upper limit on the optical depth of an OVII (OVIII) edge of 0.13 (0.12). This makes such a model unlikely (see the discussion in Sect. 4), despite an acceptable $\chi^2_{\nu}|_T = 1.04$.

If a narrow (i.e.: intrinsic width equal to 0) Gaussian line is instead employed to model the “bump” in the residuals around 1 keV, the improvement in the quality of the fit is much less, albeit formally still highly significant ($\Delta\chi^2 = 15$, corresponding to chance occurrence likelihood of $\sim 1.5 \times 10^{-5}$), with best fit parameters: $N_{\text{H}} = 2.07 \pm_{0.14}^{0.13} \times 10^{20}$ cm $^{-2}$; $\Gamma_1 = 2.17 \pm_{0.06}^{0.04}$; $\Gamma_2 = 2.761 \pm_{0.012}^{0.011}$; $E_{\text{break}} = 1.51 \pm_{0.16}^{0.12}$ keV; $E_{\text{line}} = 0.97 \pm_{0.04}^{0.05}$ keV; $EW_{\text{line}} = 16 \pm_7^6$ eV.

An alternative explanation for the relatively poor fit of the broken power-law model is that the intermediate X-ray spectrum undergoes a gradual and smooth steepening with energy, which cannot be described by an abrupt (and unphysical) switch in the spectral photon index. A gradual steepening with energy on the other hand agrees with the Synchrotron Self Compton

Table 2. Best-fit spectral parameters

Photoelectric absorbed power-law model							
Phase	N_{H} (10^{20} cm^{-2})	Γ	χ^2/dof				
A	3.83 ± 0.11	2.718 ± 0.018	839/450				
B	3.84 ± 0.08	2.643 ± 0.012	1333/531				
T	$3.80 \pm_{0.05}^{0.06}$	$2.660 \pm_{0.009}^{0.010}$	1833/561				
Photoelectric absorbed broken power-law model							
Phase	N_{H} (10^{20} cm^{-2})	Γ_1	Γ_2	E_{break} (keV)	χ^2/dof		
A	$1.9 \pm_{0.3}^{0.2}$	$2.10 \pm_{0.09}^{0.10}$	$2.82 \pm_{0.03}^{0.02}$	$1.28 \pm_{0.11}^{0.13}$	474/448		
B	$2.03 \pm_{0.16}^{0.18}$	$2.11 \pm_{0.07}^{0.06}$	$2.734 \pm_{0.013}^{0.015}$	$1.39 \pm_{0.09}^{0.11}$	640/529		
T	$1.98 \pm_{0.12}^{0.13}$	2.11 ± 0.05	$2.756 \pm_{0.012}^{0.011}$	1.35 ± 0.07	716/559		
Photoelectric absorbed broken power-law + 2 absorption edges model							
Phase	N_{H} (10^{20} cm^{-2})	Γ_1	Γ_2	E_{break} (keV)	E_{th} (keV)	τ	χ^2/dof
A	1.7 ± 0.2	2.02 ± 0.08	$2.96 \pm_{0.03}^{0.04}$	$1.57 \pm_{0.13}^{0.11}$	$1.25 \pm_{0.06}^{0.08}$	$0.25 \pm_{0.10}^{0.09}$	425/445
					1.56^\dagger	$0.19 \pm_{0.12}^{0.11}$	
B	$1.80 \pm_{0.15}^{0.17}$	$2.00 \pm_{0.06}^{0.07}$	2.87 ± 0.03	$1.65 \pm_{0.10}^{0.13}$	$1.26 \pm_{0.10}^{0.12}$	0.19 ± 0.07	531/525
					$1.60 \pm_{0.05}^{0.18}$	0.22 ± 0.08	
T	$1.77 \pm_{0.12}^{0.13}$	2.01 ± 0.05	$2.88 \pm_{0.03}^{0.02}$	$1.60 \pm_{0.12}^{0.04}$	$1.23 \pm_{0.07}^{0.08}$	$0.18 \pm_{0.05}^{0.06}$	561/554
					1.56 ± 0.11	0.22 ± 0.06	
Photoelectric absorbed variable curvature power-law model							
Phase	N_{H} (10^{20} cm^{-2})	Γ_{E}	Γ_{H}	E_0 (keV)	χ^2/dof		
$\beta = 1.0$							
A	$1.8 \pm_{0.3}^{0.2}$	$2.00 \pm_{0.12}^{0.10}$	$2.73 \pm_{0.03}^{0.02}$	1.9 ± 0.9	436/447		
B	$2.04 \pm_{0.17}^{0.16}$	2.07 ± 0.07	$2.66 \pm_{0.02}^{0.03}$	2.8 ± 0.6	553/529		
T	1.93 ± 0.13	2.04 ± 0.04	2.664 ± 0.014	2.3 ± 0.5	601/558		
$\beta = 0.3$							
A	$1.5 \pm_{0.3}^{0.2}$	$1.3 \pm_{0.3}^{0.2}$	$2.75 \pm_{0.03}^{0.04}$	$2.9 \pm_{0.7}^{1.1}$	430/447		
	1.64^\dagger	1.45^\dagger	2.77 ± 0.03	$3.5 \pm_{0.4}^{0.5}$	431/449		
B	$1.74 \pm_{0.17}^{0.18}$	$1.53 \pm_{0.15}^{0.14}$	$2.70 \pm_{0.03}^{0.05}$	$4.8 \pm_{1.2}^{2.8}$	529/529		
	1.64^\dagger	1.45^\dagger	2.69 ± 0.02	$4.2 \pm_{0.3}^{0.4}$	530/529		
T	$1.64 \pm_{0.13}^{0.14}$	$1.45 \pm_{0.13}^{0.11}$	2.70 ± 0.02	$3.7 \pm_{0.7}^{0.9}$	568/568		

† fixed

(SSC) scenario, which is nowadays widely accepted to explain the Spectral Energy Distribution (SED) of BL Lac objects (Ghisellini, Maraschi & Treves 1985; Ghisellini 1989). We have therefore parameterized the gentle concave curvature in the spectra with the function:

$$F(E) = E^{-f(E)\Gamma_{\text{H}} - [1-f(E)]\Gamma_{\text{E}}}$$

where $f(E) = [1 - \exp(-E/E_0)]^\beta$, Γ_{E} and Γ_{H} are the low and high energy asymptotic slopes and β is a ‘‘curvature radius’’ in the energy space. This model has only one degree of freedom more than the simple broken power-law. This model has already successfully fit the BeppoSAX spectrum of PKS 2155–304

(Giommi et al. 1998). It was impossible to obtain a significant constraint on β from the fitting, the nominal best fit value being $\simeq 0.30$ for all datasets. In Table 2 the results for $\beta = 0.3$ and $\beta = 1$ are shown. The former case is strongly favored from the statistical point of view and will be therefore discussed in the following. The χ^2_{ν} is comparable with that from the broken power-law + edges model for all datasets ($\chi^2_{\nu}|_T = 1.02$; $\chi^2_{\nu}|_A = 0.96$; $\chi^2_{\nu}|_B = 1.00$). The asymptotic spectral indices are $\Gamma_1 \simeq 1.45$ and $\Gamma_2 \simeq 2.70$, with a folding energy $E_0 \simeq 3.7$ keV. Interestingly, the best-fit absorbing photoelectric column density ($N_{\text{H}} \simeq 1.64 \times 10^{20} \text{ cm}^{-2}$) is

well consistent with the Galactic contribution along the line of sight to Mkn 421 ($N_{\text{HGal}} = 1.6 \times 10^{20} \text{ cm}^{-2}$, Dickey & Lockman 1990). The average 0.1–2 keV and 2–10 keV fluxes are $1.76 \times 10^{-10} \text{ erg cm}^{-2} \text{ s}^{-1}$ and $9.0 \times 10^{-11} \text{ erg cm}^{-2} \text{ s}^{-1}$, corresponding to rest frame luminosities of 7.4 and $3.9 \times 10^{44} \text{ erg s}^{-1}$, respectively.

Using this physically reasonable description of the continuum, both in the time averaged and intensity resolved spectra, the next step is to understand which model parameter(s) (and therefore which physical quantities) can be considered responsible for the spectral changes observed in Mkn 421. If all the parameters are left free, there is a suggestion that Γ_{H} and E_0 vary between Phase A and B spectra, but they are still marginally consistent within the statistical uncertainties. The fits on the intensity resolved spectra were therefore repeated, after fixing the other two parameters (i.e.: N_{H} and Γ_{E}) to their best-fit values obtained from the time averaged spectrum fitting. The asymptotic high energy slopes are different at the 90% confidence level, while the folding energies are still consistent. However, whatever the detailed reason for the spectral change is, it is what happens above $\simeq 4$ keV that determines the observed spectral variability. In Fig. 5 the best-fit model and residuals are shown for all the datasets.

Narrow-band features such as Gaussian lines, absorption edges or saturated absorption lines were added to the best-fit power-law with variable curvature model. The largest improvement in fit quality is obtained in the last case ($\Delta\chi^2 = 2.6$ for 2 degrees of freedom, which is significant at the 90% level of confidence only), with centroid energy $E_{\text{notch}} \simeq 0.55$ keV. If the notch energy is held fixed at 0.654 keV (L_{α} resonant absorption of OVIII), following the discovery of such feature in the *Einstein* spectra of several BL Lac objects (Canizares & Kruper 1984; Madejski et al. 1991), only a 90% upper limit of 10 eV on the EW can be set.

4. Discussion

Since the detection of this source at TeV energies (Punch et al. 1992), and the observation of correlation in the flaring activity at X-ray and TeV energies, observations of Mkn 421 at X-rays have become more important. The temporal coincidence of flaring in X-ray and TeV supports emission models where both components are produced by the same population of electrons with the X-rays at the endpoint of the Synchrotron spectrum and the γ -rays at the endpoint of an inverse Compton spectrum (Takahashi et al. 1996). This is consistent with the overall picture drawn from the SED of Mkn 421 which is characterized by two maxima, one in the UV/soft X-ray band, and the second at GeV to TeV energies.

There is strong evidence that the X-ray spectrum of High-energy peaked BL Lac objects (HBL) is concave (Sambruna et al. 1994; Tashiro et al. 1995; Takahashi et al. 1996; Sambruna et al. 1997). However, even the “standard” broken power-law model is unable to reproduce the spectral curvature of Mkn 421 observed here. A system of two absorption edges, whose threshold energies are broadly consistent with highly

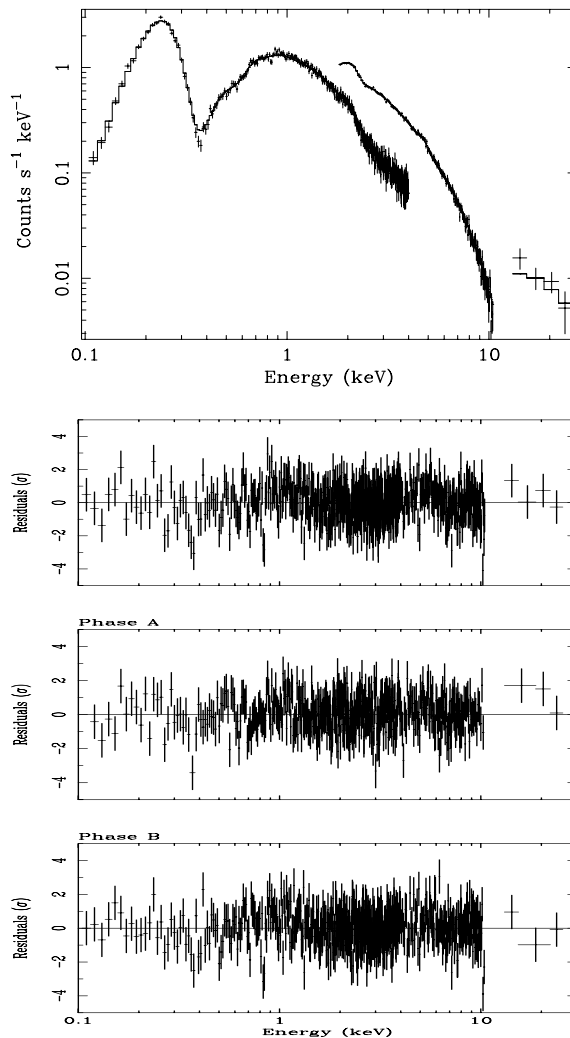


Fig. 5. Spectra and best-fit model when a photoelectric absorbed power-law with a gradually changing spectral index is applied to the time-averaged spectrum of all the instrument simultaneously (*upper panel*). The other panels show the residuals in units of standard deviations when this model is applied to the time-averaged (*upper middle*), Phase A (*lower middle*) and Phase B (*lower*) spectra

ionized Neon species NeIX and NeX, is needed to get an acceptable fit quality. However, if the edges represent the imprinting of a photoionized absorber along the line of sight, it is difficult to explain the presence of highly ionized Neon, while no Oxygen feature is detected. Assuming the K-shell photoionization cross section formulae from Band et al. (1990), the equivalent Neon column density inferred by the measured optical depth is $N_{\text{H}}^{\text{Ne}} \sim 4 \times 10^{22} \text{ cm}^{-2}$, assuming that the detected species represent the bulk of the elemental abundance. In a photoionized plasma with spectral index $\Gamma \sim 2$, the simultaneous presence of Ne IX and Ne X implies an ionization parameter $\xi \sim 10^2$, for which OVIII should be the dominant Oxygen ionic species (see e.g. Kallman & McCray 1982). Steeper spectra should only enhance the relative Oxygen/Neon ratio. The observational upper limit on Oxygen abundance is, however, more than one order of magnitude lower than Neon ($N_{\text{H}}^{\text{O}} < 2 \times 10^{21} \text{ cm}^{-2}$). This sce-

nario is viable only if deep Oxygen edges were detected as well. However, ROSAT found no evidence for these spectral features (Fink et al. 1991). We conclude that such a description of the observed spectrum is unphysical and can be discarded.

A good fit is obtained with a model where the spectral steepening occurs gradually, hence no additional spectral component is required. In this framework, the hardening of the spectrum with increasing flux is basically due to a change of the X-ray spectral properties above $\simeq 4$ keV.

It is generally believed that the radiation from BL Lac objects is relativistically beamed (Blanford & Rees 1978) and that the beam points directly towards the observer (Marscher 1980; Königl 1981). The shape of the spectrum and the measurement of polarization in the radio to optical bands provide the basis for the interpretation of the emission in terms of SSC models. Here emission up to X-ray wavelengths is caused by a relativistic population of electrons via the synchrotron process, while the γ -ray photons are created by inverse Compton scattering of the same electron population with the ambient photons (Bregman et al. 1990; Kawai et al. 1991). In the SSC model, the radiation output is driven by the highest energy electrons. The observed curvature of the X-ray spectrum can be explained by assuming that the jet is structured and the electron distribution is located in a smaller (inner) region of the jet with increasing energy. An increase in the synchrotron flux means an extension of the region where the high energy electrons are injected, probably in connection with increased activity of the nuclear engine. Alternatively, the hardening of the spectrum with increasing X-ray flux could be due to the injection of new electrons in the jet, which are highly energetic and therefore produce a flatter spectrum before they suffer significant radiative losses.

Einstein observations of a small sample of X-ray bright BL Lac objects indicate that an absorption feature at 0.65 keV may be a ubiquitous feature in their soft X-ray spectra (Majedski et al. 1991). This feature was first claimed to be detected by Canizares & Kruper (1984) in PKS 2155–304. It was interpreted as Ly α resonance absorption in OVIII ($E = 654$ eV). However, ROSAT observations (Fink et al. 1991) of Mkn 421 found no evidence for such a spectral feature. The BeppoSAX observation of PKS 2155–304 did not detect such a feature either (Giommi et al. 1998), casting further doubts on its existence in BL Lac objects. In agreement with these findings, our data show no evidence for any spectral features in the spectrum of Mkn 421. In particular no absorption feature is observed around 0.6 keV, the 90% upper limit on the equivalent width of a Ly α resonance absorption in OVIII being only 10 eV.

5. Conclusions

We summarize the main results of the presented BeppoSAX observations of Mkn 421 as follows:

- Mkn 421 was observed in a quiescent state, with an average 2–10 keV flux of 9.0×10^{-11} erg cm $^{-2}$ s $^{-1}$. It exhibited flux variation by a factor $\simeq 2$ on timescales as short as a few 10^4 s
- an energy threshold between different variability patterns can be set at $\simeq 3$ –4 keV. The 3–10 keV vs. 0.1–3 keV HR increases with increasing flux up to $\simeq 8 \times 10^{-11}$ erg cm $^{-2}$ s $^{-1}$ and then “saturates” to a constant level
- the average 0.1–40 keV spectrum exhibits a gradual steepening with energy. This effect is foreseen by the SSC scenario, where the X-rays originate as synchrotron radiation from a relativistic population of electrons in the jet. If the proper (albeit admittedly phenomenological) continuum model is adopted, no soft X-ray absorption feature is required, with a 10 eV upper limit on the equivalent width of any Ly α resonance absorption line
- the observed spectral dynamics can be explained as a hardening of the high-energy (*i.e.*: $\gtrsim 4$ keV) spectrum, above a relatively invariant soft X-ray emission. This can be due to an increase of the injected electron flux or of the extension of the injection region, possibly in connection with phases of higher nuclear activity.

Acknowledgements. MG acknowledges an ESA research fellowship. BeppoSAX is a joint Italian-Dutch program. The authors thank Dr. G. Matt for providing its XSPEC gradually changing index power-law model. Marco Beijersbergen made an invaluable contribution to the determination of the LECS response by adapting his XMM ray-trace to the BeppoSAX optics.

References

- Band I.M., Trzhaskovskaya M.B., Verner D.A., Yakovlev D.G., 1990, A&A 237, 267
- Blandford R., Rees M.J., 1978, In: Wolfe A.M. (ed.) Pittsburgh Conference on BL Lacs Objects. Univ. Pittsburgh Press, Pittsburgh, 328
- Boella G., Perola G.C., Scarsi L., 1997a, A&AS 122, 299
- Boella G., Chiappetti L., Conti G., et al., 1997b, A&AS 122, 372
- Bregman J.N., Glassgold A.E., Huggings P.J., et al., 1990, ApJ 352, 574
- Canizares C.R., Kruper J., 1984, ApJ 278, L99
- Comastri A., Fossati G., Ghisellini G., Molendi S., 1997, ApJ 480, 534
- Cusumano G., Mineo T., Guainazzi M., et al., 1998, A&A submitted
- Dickey J.M., Lockman F.J., 1990, ARA&A 28, 215
- Fink H.H., Thomas H.C., Hasinger G., et al., 1991, A&A 246, L6
- Frontera F., Costa E., Dal Fiume D., et al., 1997, A&AS 122, 357
- George I.M., Warwick R.S., McHardy I.M., 1988, MNRAS, 235, 787
- Ghisellini G., 1989, MNRAS 236, 341
- Ghisellini G., Maraschi L., Treves A., 1985, A&A 146, 204
- Giommi P., Barr P., Garilli B., Maccagni D., Pollock T., 1990, ApJ 356, 432
- Giommi P., Fiore F., Guainazzi M., et al., 1998, A&A 333, 5
- Harmon B.A., Finger M.H., Rubin B., et al., 1992, In: Shrader C.R., Gehrels N., Dennis B. (eds.) Proceedings of the Compton Observatory Science Workshop. NASA CP3137, 69
- Kallman T., McCray R., 1982, ApJS 50, 263
- Kawai N., Matsuoka M., Bregman J.N., et al., 1991, ApJ 382, 508
- Königl A., 1981, ApJ 243, 700
- Kubo H., Takahashi T., Madejski G., et al., 1998, ApJ 504, 693
- Lampton M., Margon B., Bowyer S., 1976, ApJ 208, 177
- Lin Y.C., Bertsch D.L., Dingus B.L., et al., 1996, A&AS 120, 499
- Macomb D.J., Akerlof C.W., Aller H.D., et al., 1995, ApJ 449, 99

- Madejski G.M., Mushotzky R.F., Weaver K.A., Arnaud K.A., 1991, *ApJ* 370, 198
- Manzo G., Giarrusso S., Santangelo A., et al., 1997, *A&AS* 122, 341
- Marscher A.P., 1980, *ApJ* 235, 386
- Parmar A., Martin D.D.E., Bavdaz N., et al., 1997, *A&AS* 122, 309
- Punch M., Akerlof C.W., Cawley M.F., et al., 1992, *Nat* 358, 477
- Ricketts M.J., Cooke B.A., Pounds K.A., 1976, *Nat* 259, 546
- Sambruna R.M., Barr P., Giommi P., et al., 1994, *ApJS* 95, 317
- Sambruna R.M., George I.M., Madejski G., et al., 1997, *ApJ* 482, 774
- Tashiro M., Makishima K., Ohashi T., et al., 1995, *PASJ* 47, 131
- Takahashi T., Tashiro M., Madejski G., et al., 1996, *ApJ* 470, 89
- Ubertini P., Bazzano A., La Padula C., Polcaro V.F., Manchanda R.K., 1984, *ApJ* 284, 54